Chapter 42
Computational Analysis: A Bridge to Translational Stroke Treatment

Nirmalya Ghosh, Yu Sun, Christine Turenius, Bir Bhanu, Andre Obenaus, and Stephen Ashwal

Abstract Objective rapid quantification of injury using computational methods can improve the assessment of the degree of stroke injury, aid in the selection of patients for early or specific treatments, and monitor the evolution of injury and recovery. In this chapter, we use neonatal ischemia as a case-study of the application of several computational methods that in fact are generic and applicable across the age and disease spectrum. We provide a summary of current computational approaches used for injury detection, including Gaussian mixture models (GMM), Markov random fields (MRFs), normalized graph cut, and K-means clustering. We also describe more recent automated approaches to segment the region(s) of ischemic injury including hierarchical region splitting, support vector machine, a brain symmetry/asymmetry integrated model, and a watershed method that are robust at different developmental stages. We conclude with our assessment of probable future research directions in the field of computational noninvasive stroke analysis such as automated detection of the ischemic core and penumbra, monitoring

N. Ghosh (✉) • C. Turenius, PhD • S. Ashwal, MD
Department of Pediatrics, Loma Linda University, Loma Linda, CA, USA
e-mail: NGhosh@llu.edu

Y. Sun, PhD • B. Bhanu, PhD
Center for Research in Intelligent Systems, University of California, Riverside, CA, USA

A. Obenaus, PhD
Department of Pediatrics, Loma Linda University, Loma Linda, CA, USA

Department of Radiology, Loma Linda University, Loma Linda, CA, USA

Department of Radiation Medicine, Loma Linda University, Loma Linda, CA, USA

Department of Biophysics and Bioengineering, Loma Linda University, Loma Linda, CA, USA

P.A. Lapchak and J.H. Zhang (eds.), *Translational Stroke Research*, Springer Series in Translational Stroke Research, DOI 10.1007/978-1-4419-9530-8_42,

of implanted neuronal stem cells in the ischemic brain, injury localization specific to different brain anatomical regions, and quantification of stroke evolution, recovery and spatiotemporal interactions between injury volume/severity and treatment. Computational analysis is expected to open a new horizon in current clinical and translational stroke research by exploratory data mining that is not detectable using the standard "methods" of visual assessment of imaging data.

1 Introduction

Focal and global cerebrovascular insults remain a common and devastating disorder in adults and children. The last 2 decades have seen a rapid progression of scientific and clinical advances due in large part to the implementation and application of neuroimaging, including magnetic resonance imaging (MRI), computed tomography (CT), and positron emission tomography (PET). Numerous reviews (including chapters in this book) highlight the importance of neuroimaging for diagnosis and assessment of therapeutic effectiveness [1, 2]. Visual assessment is used primarily to guide clinical decisions for patient care, but what is lacking in clinical and experimental studies is the ability to rapidly extract quantitative data. We summarize the current state of computational analytical approaches particularly, as they apply to MRI to evaluate focal and global cerebrovascular injuries. Although substantial information can be acquired from visual assessment of MR images, it is readily apparent that application of computational analytical methods can have substantial clinical usefulness (Table 42.1). Since these computational advances provide rapid and quantitative data, they may assist clinicians in treatment decisions including which patients may be candidates for specific treatments and to assess where in the brain particular treatments could be targeted (e.g., location of stem cell implantation or drug injection). Our research efforts have focused on newborns with global or focal ischemic injuries in experimental animal model systems, as well as in term neonates. However, the computational approaches we describe have broad applicability across a spectrum of ages and diseases.

Application of computational assessments to translational stroke research can be separated into the following sequential steps: (a) detection of injury and extraction

Table 42.1 Benefits of computational methods in cerebrovascular disease

Minimize or eliminate observer bias for lesion detection
Objective quantification of lesion volume compared to manual methods
Ability to rapidly acquire computational results compared to manual methods
Ability to quantitatively and serially determine changes in lesion volume and extent
Differentiate ischemic core from penumbra
Quantify regional anatomical injury severity (by use of templates and parcellation)
Quantify evolution of injury over space and time
Quantify injury–treatment interaction and recovery over space and time
Utilizing these information in candidate and treatment selection for therapeutics

of lesion volume, (b) estimation of a lesion's core and penumbra, (c) quantification of a lesion's region-specific information based on anatomy, (d) target drug treatment or other therapeutic advances (e.g., implantation of neural stem cells: NSC), (e) detection of implanted MR-labeled stem cells, (f) serial imaging and monitoring of the interaction(s) between the stroke lesion and treatment effects in space and time, and (g) analyzing treatment effectiveness on tissues associated with a lesion. Computational methods based on image processing, computer vision, machine learning, and pattern recognition techniques have the ability to improve data accuracy and yield clinically relevant information. The contents of this chapter are focused on current automated methods that are limited primarily to lesion detection but also describe several recent approaches to lesion quantification including estimation of core–penumbral tissues. We have also applied some of these computational approaches to monitoring of implanted stem cells in experimental models. Finally, we explore several different approaches to future research using brain atlases for anatomy-specific spatiotemporal monitoring of stroke and stem cell interactions.

2 Current Computational Approaches for Lesion Detection

Visual and manual lesion assessments which are commonly used [1, 3–6] suffer from the misperception of contrast due to the parallax effects of neighboring pixels/voxels—pixels with the same intensity values may look different due to its neighboring pixels [7, 8]. Issues such as user fatigue related errors in time-consuming manual assessment methods and intra- and interobserver variability potentially compromise data comparisons. Simplified semiquantitative scoring systems to grade injury severity have been useful in grading injury severity in clinical patients (e.g., [9–12]) and in experimental models (e.g., rat pup severity score, RPSS [13]). Although useful, these simplified scores are grossly subjective and only qualitatively measure the extent of injury. Unfortunately, they do not provide objective and accurate quantification of injury volumes. Some investigators have developed automated lesion segmentation methods that use manual thresholds [14], cross-correlations based on ad hoc templates [15], Otsu's algorithm [16] on similarity maps of intensity and proximity [17], or use manually derived percentage of maximum values from apparent diffusion coefficient (ADC) maps in neonates with stroke [6, 18]. In most cases, these approaches are ad hoc and are not robust to MR signal and noise level variations across different datasets. What has not been developed are computational methods, based on reliable mathematical models that objectively analyze medical images in a reproducible, quantifiable, and accurate manner at near real time speed.

Some computational methods have been developed for other diseases such as multiple sclerosis (MS) [19, 20], focal cortical dysplasias (FCD) [21, 22], and white matter lesions (WML) [23]. Since these methods use MRI signal contrast to detect abnormalities, they can be modified or extended to evaluate lesion characteristics

seen with ischemia or stroke [23, 24]. Reviewed below are some of the different available approaches, focused on automated methods such as GMMs [25], MRFs [26], normalized graph cut [27], and K-means clustering [28] for the detection of brain abnormalities. Although many of these methods have considerable similarities and are sometimes indistinguishable, we describe them separately.

2.1 Gaussian Mixed Models

MR signal intensity of similar brain tissues are expected to be the same. Image noise, including the noise within MR images is primarily Gaussian in nature. This and the central limit theorem [29] (which states that, as the number of data points increase toward infinity, the distribution of data points gradually becomes close to Gaussian) imply that different tissues, such as gray matter (GM), white matter (WM), cerebrospinal fluid (CSF), or lesioned tissues, are expected to aggregate under different Gaussian curves with their means distinctly separated for easy differentiation. Each pixel/voxel has a particular probability to be classified as WM, GM, CSF, or lesion, and the highest probability defines the tissue type of the pixel/voxel. These variations within tissues are modeled by a GMM where every pixel/voxel is represented as a weighted sum of Gaussian distributions parameterized by (a) weights (or prior probability), (b) means, and (c) standard deviations of the individual Gaussian (i.e., tissue) components. With appropriate selection of the MRI modality and tissue types, a training set of data can be used to learn these parameters by use of an Expectation-Maximization (EM) algorithm [7]. EM iteratively modifies the parameters namely weights, means and standard deviations of the Gaussian distributions to fit the training data for which the tissue class of each pixel/voxel is known. In other words, the EM algorithm maximizes the expectation that the data came from the estimated GMM model. A key research focus has been on automated MRI segmentation of brain anatomical structures (GM, WM, and CSF) using GMM and its derivatives (e.g., constrained GMM; CGMM). Greenspan and colleagues have used a CGMM where global intensity with local spatial characteristics has been used with EM based parameter learning [30]. Connected component based top-down splitting of the MR regions is done to get tissue classes (WM, GM, and CSF) having different mean MR intensities. As GMM does not utilize an atlas-based registration it can be applied to other disease states or to data where atlases are not yet available. An example of this relates to the developing neonatal brain where reliable age-matched atlases have not yet been published. These Gaussian distributions can be closely spaced, i.e., the mean MR signal intensity of different tissues are close, so that on occasion, one needs to consider fuzzy connectedness where class membership values are like weights in GMM but with "fuzzyness," in which the probabilities of a voxel being in tissue A and tissue B are assigned [31]. However, histogram fitting to a normalized histogram, as adapted by Fan and colleagues, cannot be used when large lesions affect the shape of the histogram [32].

In some cases, the lesion has been modeled as a "reject" class in normal tissue models (GM, WM, CSF) where the voxels, not satisfying the GMMs derived from the EM algorithm, are detected as lesion [33]. Agam and colleagues have used a mixture-parametric probabilistic model where optimized parameters are found by EM-based incomplete log-likelihood maximization for detecting chronic stroke lesions [24]. Probabilistic priors are computed from registered control data sets and deviation from these priors in multimodal fused data sets (T1, T2, and diffusion tensor imaging (DTI)) is used to detect the lesion. A key disadvantage of GMM based methods is that they break down in analysis of imaging data with a magnetic bias field (an unwanted baseline magnetic field in the MRI scanner) as this shifts the Gaussian means of the tissues linearly or nonlinearly leading to incorrect tissue classification. Bias field correction methods can reduce such problems [27]. Also GMM suffers badly when there are data with large voxel sizes, such as magnetic resonance spectroscopy (MRS), where partial volume effects may affect classification of voxels in tissue borders. Superresolution methods could be used to improve performance [34].

2.2 Markov Random Fields

In Markov models, the data points (e.g., MRI voxels or regions) and their different possible classes (e.g., WM, GM, CSF, lesion) are represented as nodes of a graph where links between the nodes carry a probabilistic association for each data point to different classes. MRFs are generally multidimensional where the connected lines of the graph are not directed. Tissue types classified as normal/abnormal or WM–GM–CSF (or some other user-based classification) are designated as nodes. Voxel nodes are defined as the observed variables while tissue nodes are the estimated or hidden classes. Association of voxel nodes to different classes are controlled by joint probability distributions (i.e., probability of a particular voxel being classified as a particular tissue) and represented by lines connecting these nodes. Atlas prior probabilities and MRFs have been used to discard partial volume effects and reduce outliers in patients with multiple sclerosis lesions [33]. Kabir and colleagues have used multimodal MR data (T2, fluid attenuated inversion recovery (FLAIR), diffusion sequences) and longitudinal data (6 h, 5 and 30 days) that were coregistered to form a multimodal MRF [35]. Using this novel approach, they were able to demonstrate that in adults with stroke, the lesion distribution follows the vascular territory of an occluded blood vessel. They also generated normalized vascular territory maps that could be utilized for stroke classification and improved clinical interventions. The significance of their work is that they demonstrated that stroke territories shift over time. Hidden Markov models (HMM), a variant of multidimensional MRF, have been used to find WM–GM–CSF tissue types [26]. In another recent study, 3D Hilbert–Peano mapping was used to convert 3D T1 and FLAIR data into 1D data for computational ease [19]. A 1D MRF (Hidden Markov Chain; HMC) was then used in the preprocessing step to account for neighborhood information to improve intratissue signal homogeneity and intertissue signal

contrast. A likelihood estimator was then used to prune and detect regions not falling in any of the tissue class (outliers) to identify the lesion as an MS lesion. Finally a probabilistic tissue atlas was used to reject false detection.

As the number of MR regions and tissue classes increase, the complexities of the joint probability distributions in MRF become intractable. Often prior knowledge that a particular type of lesion is only localized to a certain brain region simplifies the connectivity of the graph and the associated joint distributions. Similarly, an MR region highly associated with a tissue class (e.g., CSF) precludes its possible association with another tissue class (e.g., GM), as generally they are not adjacent. This type of prior knowledge leads to probabilistic conditional independence with a known condition, as one MR region cannot be associated with different tissue or anatomy classes. This brings about cause and effect relations between graphical nodes and removes some of the connected links in the MRF (based on conditional independence).The remaining links are manifested as arrows pointing from a "cause" node to an "effect" node of the graph. Bayesian networks (BNs) are such a probabilistic graphical model with directed acyclic graphs (DAG) [36]. BNs also have been used to find abnormal tissues [37]. In these cases, network parameters (e.g., which region(s) are connected to which tissue type) are to be learned from training data sets with manually derived tissue classification available for each MR voxel/region [36].

2.3 Normalized Graph Cuts

In MR images, voxels with similar signal intensity form regions. The similarity or contrast of signal (i.e., coherence or difference) defines how strongly two voxels are alike (or different). Based on such intervoxel signal comparisons, an MR image can be represented as a graph with each pixel/voxel as a node of the graph and connecting (undirected) lines are weighted to represent how strongly the two voxels are similar (i.e., from the same tissue class). The strengths of these links are computed from the similarity in features of corresponding voxels, such as MR signal intensity, texture (in a close neighborhood), and location proximities. This graph can be represented as a multidimensional matrix and its Eigen vectors can be computed by singular value decomposition (SVD). Based on graph mathematical theory, the second weakest Eigen vector, sometimes called "Fiddler vector," defines the "weakest link" between two strongly connected "subgraphs" [38], for example a separating plane between WM and GM tissue types in T1/T2 weighted MRI. If we apply normalized graph cuts (N-Cut) for solving MRFs, the basic graph cut algorithm ensures near global minimum of the energy function of the MRF. As N-Cut algorithms often suffer from oversegmentation due to artifacts and noise, age-matched control atlases or probabilistic tissue models can be useful [27]. Such prior tissue models and N-Cut methods have been used to separate WM, GM, and CSF regions where iterative algorithms alternate between N-Cut based segmentation and atlas based inhomogeneity corrections. In other words, small outlier regions that are detected inside large correctly classified tissue (due to signal inhomogeneity) are modified to have a better match with the atlas.

2.4 K-Means Clustering

GMM and MRF typically require training datasets with manually detected lesions (ground truth) to assist in supervised learning. When such ground truths are not available, unsupervised learning can be used by evaluating MR image clusters based on the cohesiveness of voxel features such as MR signal intensity, location, texture, etc. Cluster cohesiveness can be measured as the ratio between the intracluster standard deviation and the intercluster mean distances, that is, how distant the clusters are from each other [29]. Freifeld and colleagues have used K-means clustering to detect multiple sclerosis lesions from T2-weighted images [25] where they have used a multimodal approach, starting with CGMM-based initial grouping of tissue types (WM, GM, CSF) that iteratively split the tissue regions [30]. Then they have used expert rule based and multimodal fusion of MR images (T1, T2, and proton density MRI) to robustly identify small lesions. Since multimodal fusion often blurs the boundaries between the regions they utilized active contours to sharpen the boundaries.

In some instances, after CGMM based initial tissue segmentation, deformable models along with K-means clustering have been used to improve MRI tissue classification within the brain so as to generate a tissue type atlas [28]. In these heavily model driven approaches, lesions of a known shape can be readily identified if the lesion encompasses an entire brain region (e.g., putamen) but this approach does not work when the lesions cross anatomical boundaries, as is the case in the majority of stroke patients. When data clusters are too close to one another, partial or fuzzy association to neighboring clusters (i.e., classes) can be used, just like the previously described fuzzy concept in the GMM approach. Spatially constrained fuzzy kernel clustering methods have been used to estimate MR bias fields, which need to be corrected for improved brain atlas generation or GMM-based lesion detection [39]. This also accelerates the usually slow kernel-clustering method in high dimensional feature space [39]. Before applying these types of bias correction methods, it should be kept in mind that in some situations, small lesions can be classified as an artifact and hence removed as an outlier. Fuzzy clustering has also been used to detect gray matter atrophy in MS lesions using a fusion of probability maps (from brain morphology), signal intensity (from MRI), and brain anatomy (from atlas) [40]. A similar method, K-nearest neighbor method, has been used for WM–GM–CSF classification after tissue probability models or atlases were registered to the data [23]. The MRI was intensity-rescaled after truncating high-low outliers. WM lesions were detected from the histogram of the WM only.

2.5 Other Methods

Lesion detection can be improved by preprocessing the MR images using spatial regularization or congruity by MRI textures [41, 42], probabilistic models [24], morphological operations [43], and physical model estimation [44]. In some instances, multiple MRI modalities can be used sequentially to achieve better

insights into the clinical relevance of the imaging abnormalities. Dugas-Phocion and colleagues used EM based temporary grouping of tissue types (WM, GM, CSF), thresholded the voxel-wise MR signal differences to find supratentorial MS lesions in T2 FLAIR, and then proposed T1/T2 lesion differences as the possible internal structure of the lesion [20]. They registered all the modalities for voxel wise comparisons. For multimodal fusion, a key requirement is coregistration to a standard space which often severely suffers when different modalities have different resolutions. For example, functional MRI (fMRI) data or MRS derived metabolite ratios in different anatomical brain regions are often acquired at a coarse resolution (i.e., large voxel size) compared to T1 or T2 anatomical data [45]. The common method of down sampling high resolution T1/T2 data and working on the coarse functional space is relatively simple but associated with loss of small variations due to the large voxel size. Attempts have been made to improve the resolution of fMRI to overlay onto high resolution anatomical spaces using ad hoc methods [45]. Application of superresolution technologies that have been used in the computer vision field may help to overcome partial volume effects when merging low to high resolution MR data [34].

3 Recently Emerging Approaches for Automated Lesion Detection

Several disadvantages of current approaches to lesion detection have hampered their widespread translational use. First, computationally intensive mathematical models are generally used that hinder rapid estimation of the size and nature of the lesion which is time sensitive when used clinically [19, 21, 25, 30, 39]. Second, many current methods use anatomical brain atlases and a priori probabilistic tissue models [23] to facilitate lesion detection and reject outliers [19, 33]. However, neither atlases nor probabilistic models are always statistically valid for the data being evaluated (e.g., stroke data may have distortions and structural uniqueness that cannot be mapped well to an atlas) and may lose information during spatial registration of the injured brain to the atlas brain. Since ischemic and stroke lesions often cross anatomical boundaries, the use of modeling or atlases or priors is likely not justified. In addition, none of the current research has the capability of analyzing the internal structure of an ischemic/stroke lesion which ultimately may be relevant for clinical treatment decision making (see [20] for an exception). Finally, compared to other neurological disorders, there has been little research dedicated to automated detection and quantification of ischemic injury [35].

3.1 Hierarchical Region Splitting

Hierarchical region splitting (HRS) is an automated region segmentation method that splits MR images recursively to generate a binary tree-like structure (Fig. 42.1).

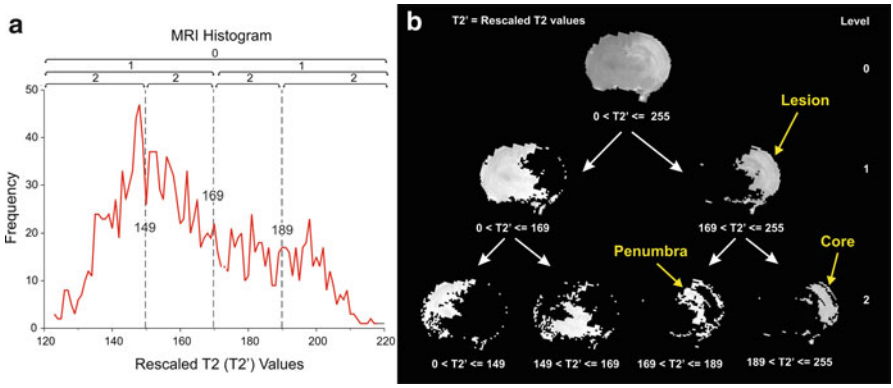

Fig. 42.1 HRS methodology. (**a**) T2 histogram: T2WI is rescaled (T2′) to intensity range (0–255). The HRS method fits a bimodal distribution and detects a valley at $T2' = 169$ as the threshold to split the histogram. This splitting is repeated recursively (next level thresholds are $T2' = 149$ and 189). (**b**) HRS tree: Segmenting the T2WI into regions with T2′ values in these particular ranges in (**a**) form the HRS tree. Subimages in (**b**) are rescaled for enhanced visualization. HRS automatically detects the right image in Level 1 as the ischemic lesion. HRS further segments the lesion into the core and the penumbra regions in Level 2. Note that only part of the complete HRS tree is shown

The subimages are based on the uniformity and contrast in MR signal (intensity or quantitative values) that are representative of the underlying tissue characteristics (e.g., normal vs. injured brain). Recently, we have reported that HRS can detect and extract neonatal hypoxic ischemic lesion volumes, with excellent volumetric correlations ($r^2 = 0.95$; $P = 8.6 \times 10^{-7}$) and overlap (sensitivity: 0.82, specificity: 0.86, similarity: 1.47) to manually extracted results [32]. Although the methods and results of HRS were obtained from MR images, HRS is a generic method for any medical image (e.g., MRI, PET, CT) where contrast in the medical image is used to detect abnormalities.

The key steps for HRS detection of ischemic/stroke lesions (Fig. 42.1) are: (1) *MR image rescaling*: MR images are rescaled to an image intensity range [0–255] and the pixel wise conversion factors are stored to map the automatically derived results back to their original MR values or intensities. (2) *Derive image histogram*: A histogram of the MRI is computed. (3) *Compute adaptive segmentation threshold*: The image histogram is then modeled as a bimodal distribution with two distinct and distant peaks, which segregates the MR images into two different tissue regions (Fig. 42.1a). The valley between the histogram is then computed and acts as an adaptive threshold that is used to split the image into two subimage regions that have uniform image intensity or values [16]. Each histogram peak is representative of a region with a minimum intraregional image variance and a maximum interregional image variance. (4) *Recursive bimodal segmentation*: The adaptive image segmentation step is now used recursively to split each of the resultant subregions (subimages) to generate a tree-like hierarchical data structure (called HRS

Table 42.2 T2 and ADC values for tissue-types over time in rat pups

	ADC ($\times 10^{-5}$ mm^2/s)			T2 (ms)		
Age (days)[a]	NABM	1–2 days lesion	Fe-labeled NSC[b]	NABM	3–7 days lesion	Fe-labeled NSC
10–12	60–150	<40	–	30–50	>80	<20
13–17	60–120	>150	–	50–80	>100	<40
>17	60–100	>120	–	50–100	>120	<50

The MRI range of values were used as prior knowledge in HRS based stroke and stem cell detection.

[a]HII was induced at postnatal day 10, followed by serial imaging (see Obenaus et al. [73]).

[b]Iron-labeled NSC ADC values were not extracted as T2 is a more sensitive modality.

tree; Fig. 42.1b). Each segmented region at any level of the HRS tree is the MRI data within two threshold values. (5) *Criteria for stopping segmentation*: Recursive image segmentation is continued until each of the resultant subregions/subimages have uniform image intensity based on these criteria: (a) individual connected regions are small and unlikely to be partitioned further into separate subregions (i.e., different tissues); (b) the image intensity or value for each subregion has a low standard deviation value (i.e., if from MRI, uniform MR physical properties); and (c) the image histogram of the segmented region has a low kurtosis value (i.e., a sharp histogram peak that cannot be split further).

When the medical image contains bone (e.g., skull) and CSF regions, HRS can be employed using a different set of parametric values to separate these unwanted regions leaving only brain tissue for recursive splitting. Use of automated HRS avoids manual skull stripping which is time-consuming. To detect small lesions, HRS further splits the skull-stripped brain using a different set of parameters. For this, as the HRS criteria for stopping segmentation, smaller limits for area, standard deviation and kurtosis are used that provide a deep-rooted HRS tree with small subregions. Finally, HRS can use previously established normative data (from published studies or experience) to provide a generic range of image values (a) for normal appearing brain matter (NABM) and injured tissues (e.g., stroke), (b) for the particular neuroimaging modality being used (e.g., MRI T2, diffusion weighted, etc.), and (c) for the appropriate imaging time point (e.g., relevant to the time point post ischemia/stroke onset as neuroimaging values change). Because T2 relaxation and diffusion coefficient (ADC) values change with brain development or with injury, or both, they need to be adjusted for accurate lesion detection.

Based on our application of HRS in a neonatal model of hypoxic ischemic injury we have determined an approximate range of MR image values that are useful for temporal discrimination of normal appearing brain matter and lesion (Table 42.2). Means of the subregions from the HRS tree are compared with these a priori known tissue values. The subregions with their mean values within the MR property range for the injury in Table 42.2 are merged to obtain the final HRS detected lesion [32]. This is repeated for each imaging modality and at each imaging time point considered in the study. This HRS approach results in excellent HRS detected ischemic lesions (Figs. 42.1b and 42.2a) at two time points (4 and 14 days post hypoxia

ischemia). In other neurological diseases, the HRS threshold values are likely to vary; however, typically the image value ranges between NABM and abnormal regions are widely separated and can be used to automatically distinguish abnormal from normal tissue. Compared to current lesion detection approaches (see above) that depend heavily on tissue models, HRS is a generic method that adapts to any type of medical image, injury and across the age spectrum.

3.2 Support Vector Machine

At the present time, HRS has utilized only the MR signal or MR value as the primary image feature to classify pixels/voxels. However, other image features from multiple (registered) modalities such as signal intensities, textures [41, 42], proximity [17], shape indices, probabilistic indices from anatomical atlases, and prior knowledge [23] can be used to classify any voxel. The feature sets from each pixel (or region) from each MR image creates a singular data point within a multidimensional feature space.

Our ultimate goal is to define a set of image features that robustly separate ischemic/stroke volume from normal brain tissues. In mathematical terms, within the feature space, we wish to find a surface, one side of which has data points from the normal brain while the other side having data points from the lesion. The data points in both classes that are closest to separating this hyperplane are the most error prone points and define the "functional margin" [46]. Instead of defining ad hoc the location of a hyperplane, it is best to identify this separator adaptively from the data itself. One approach is to use a "training data" sample that has the features of interest, as well as a manually determined classification (e.g., stroke, NABM). Once a hyperplane or classifier is trained using a supervised learning method (e.g., EM algorithm), a new data point without any manual detection (i.e., "testing data") can be classified based on the output of the discriminating function (learned during the training phase) by determining on which side of the classifier surface the new data point falls.

Support vector machine (SVM) is one such supervised machine-learning algorithm that searches for nonlinear classifier surfaces within the feature space that separates different classes [47]. For example, after registering T2 and ADC maps of an injured brain, T2 relaxation values and diffusion coefficients are used as the voxel feature in SVM (Fig. 42.2b), and normal brain tissue, lesion core, and lesion penumbra are separated by nonlinear curves. If the feature space does not reliably separate tissue classes, different combinations of the features can be used to generate more complex features that would assist in differentiating the tissue features. This process is done by projecting current feature-set to a higher dimensional feature space using kernel functions that are nonlinear functions of the simple features such as the T2 and ADC values. The underlying assumption is that a better nonlinear hyperplane (separating tissue classes) could be learned in this new feature space. SVM attempts to maximize the "functional margin" of the hyperplane or a separation that maximizes accuracy and distance between the separating plane and

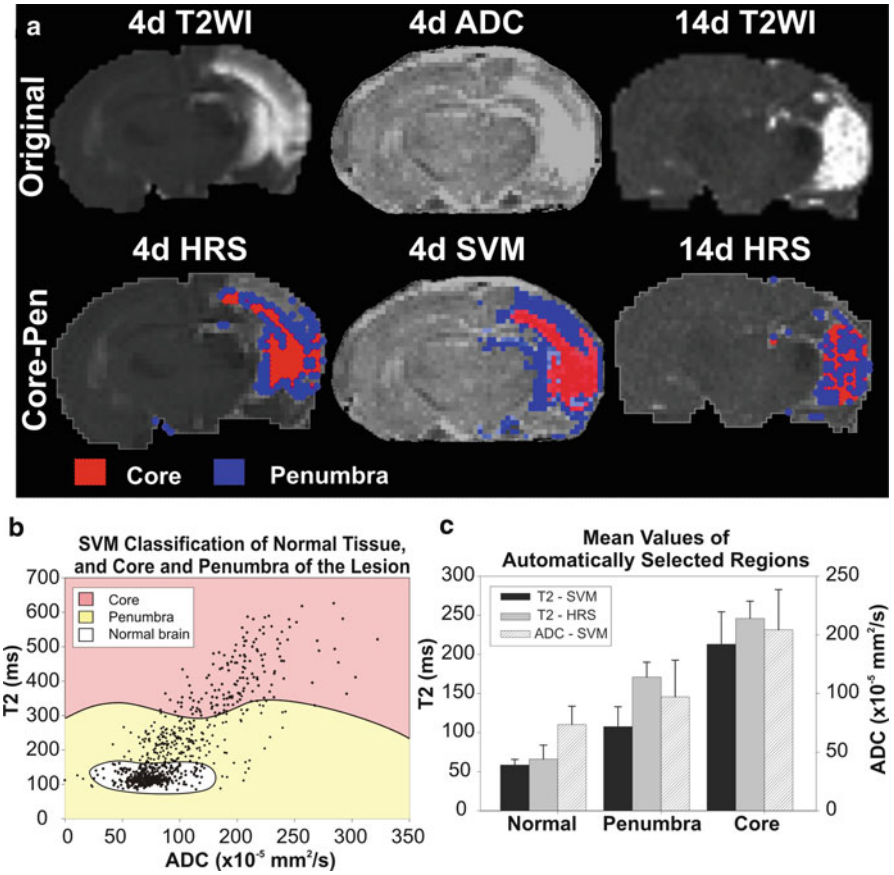

Fig. 42.2 Lesion core and penumbra detection by HRS and SVM: (**a**) HRS detected core (*red*) and penumbra (*blue*) at 4 and 14 days post ischemia using T2 maps. SVM detected core and penumbra from T2 and ADC maps (after spatial coregistration) at 4 days post injury. The core–penumbra relative percentages and locations change considerably from 4 to 14 days, illustrating a temporal evolution of the ischemic lesion. (**b**) SVM feature-space with T2 and ADC values of the voxels in 4d (post ischemia) data in (**a**) and nonlinear classification surfaces learned by segmentation of normal tissue (*white*), core (*pink*) and penumbra (*yellow*) of the lesion. (**c**) In addition to core–penumbra overlap, T2 and ADC means for normal tissues, core, and penumbra that were detected by HRS and SVM reveal excellent concordance

most data points [46], leading to improved tissue identification. Recently, SVM has been used to detect FCD from texture features derived from MRI [21]. Initially, gray matter was found by registering to an atlas and gray matter textures were derived from statistical gray level cooccurrence and "run length" features (i.e., for how many pixels/voxels the same classification continues in different image directions). In the texture space, SVM is then trained and used to separate relatively small gray matter lesions.

Higher "functional margins" would be associated with lower generalization errors in the test set. Incremental learning can then be used where classification for the test data is validated by an expert (e.g., a physician, researcher) and this feedback may be incorporated to improve the SVM classifier. At different imaging time points, different sets of features may be more effective in classifying the same tissue (normal tissue, ischemic/stroke lesion or presence of implanted stem cells). Different training data sets may be needed to train different classifiers for different time points to better extract the evolving lesion. Following coregistration of ADC and T2 maps in a neonatal model of ischemia, an SVM based classifier effectively separated the lesion from NABM as well as discriminating putative ischemic core and penumbra regions (Fig. 42.2a, b). The advantage of SVM compared to HRS lies in its ability to adaptively learn the classifier by a training set of data and to utilize multiple features (e.g., intensity, texture, shape, etc.), but at the cost of being more computationally intensive (than HRS) for training, that can limit throughput. Comparative results in Fig. 42.2a, c show that HRS and SVM detected lesion regions overlap almost identically. Thus, identification of similar regions using two completely different computational methods to detect the lesion strengthens the validity of both results. However, HRS will be more effective for single feature based classifications, whereas SVM will be more useful when multiple features are used to classify the data.

3.3 Brain Symmetry-Based Approaches

Normal brains are highly symmetric and this has been used for automated brain segmentation [48]. However, in stroke and other diseases (as well as in translational models), injury areas are often asymmetric (Fig. 42.3a), i.e., the region contralateral to a stroke is often normal, albeit with significantly different MRI signals. Asymmetry itself can be used as a prominent feature for identification of brain injuries. Examples of asymmetry detection in brain injury and disease include tumors from T2-FLAIR images [49], MS plaques from T1 and T2 weighted images [48], and FCD using textures in T1 weighted image [22].

Recent studies have reported a fully automated symmetry integrated detection method for stroke [50, 51]. Like most current automated (and manual) methods, a brain region is detected as abnormal when regional properties such as symmetry deviate from those for NABM. The regions of the brain that are not symmetric are hypothesized as the regions involved in the injury and are then further tested for the presence/absence of injury. Key steps of this approach are summarized in Fig. 42.3. From the input MR image (Fig. 42.3a), the axis of symmetry (AoS) is first estimated (Fig. 42.3b) and a "symmetry affinity matrix" (Fig. 42.3c) is computed based on intensity similarity between mirror-symmetric locations of the two sides of the AoS. A symmetry integrated region growing method is then applied to segment symmetric and asymmetric regions (Fig. 42.3d) followed by kurtosis and skewness measurements of symmetry affinity to extract the asymmetric region(s) (Fig. 42.3e). For increased robustness to variations in MRI and lesions, the symmetry affinity

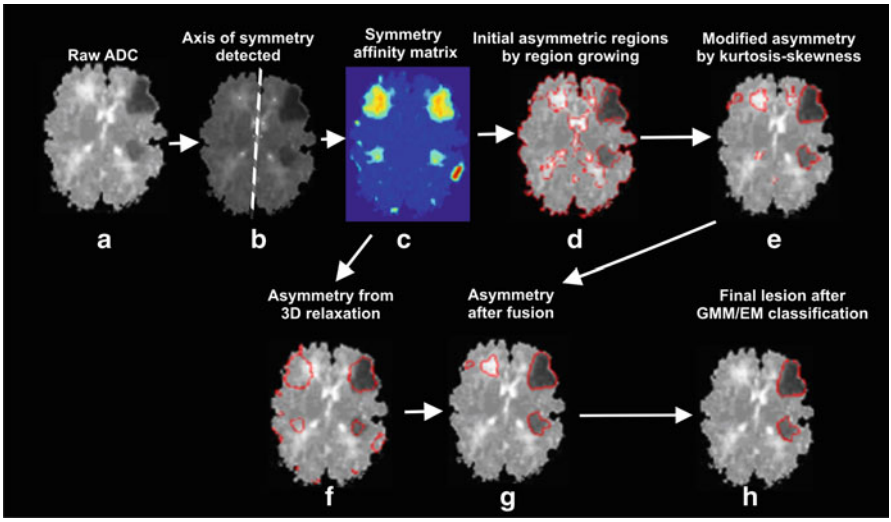

Fig. 42.3 Symmetry-based lesion detection. Results are shown of a symmetry-integrated lesion detection method in a term newborn with stroke using ADC. From (**a**) the original ADC, (**b**) the axis of symmetry (AoS) is detected (*dotted line*). (**c**) A symmetry affinity matrix is computed where brighter (*yellow*) regions are more asymmetric across the AoS. (**d**) Symmetry-integrated region-growing extracts these initial asymmetric regions (**e**) that are then modified using kurtosis–skewness measures of the regions. (**f**) Separately, asymmetric clusters are also detected from 3D gradient relaxation algorithm. (**g**) Robust asymmetric regions are computed from the fusion of the detected regions in (**e**, **f**). (**h**) Finally GMM/EM classifies the stroke regions from the asymmetric regions in (**g**)

matrix (Fig. 42.3c) is also separately processed using a 3D gradient relaxation algorithm for clustering and identification of asymmetric groups (Fig. 42.3f). The results from Fig. 42.3e, f, are then fused to obtain refined asymmetric regions (Fig. 42.3g). Finally a GMM/EM based supervised classifier is trained (from "training data") and applied to classify asymmetric regions into injured and healthy tissues using image signal intensity and 3D asymmetry volumes to quantify the stroke lesion (Fig. 42.3h). Using this approach, we found that automated symmetry identified lesion volumes varied only by an average of 7.53%, compared to manually identified lesion volumes [50, 51].

The key advantages of the symmetry method are that it is not dependent on the patient or stroke age or a priori knowledge of NABM and lesion ranges (see Table 42.2), and it does not require registration with an atlas or prior models. However, disadvantages include that it is more computationally intensive than HRS, can fail to identify an AoS when a severe injury causes bilateral hemispheric alterations, and can fail to detect injury regions if the stroke is diffused or global in nature when mirror-symmetric regions from both hemispheres are injured [32]. In these cases, other types of "prior knowledge" may be used and currently are being investigated.

3.4 Watershed-Based Segmentation Approaches

Watershed approaches to injury detection attempt to model a medical image as a topographic map and find the regional (local) maxima in the altitude as segmentation boundaries. For instance, the signal values in a brain MR image can be thought of as the altitudes on a topographic map. If a drop of water falls on this relief, it can take different paths to finally reach a local minimum, called a "catchment basin." For MRI, the lowest signal regions represent these local minima and regional maxima form the crests or watersheds. Watersheds are the limits of the adjacent catchment basins and represent the image segmentation boundaries. The path of the downward water flow in the watershed model is similar to the minimization of signal energy (from MRI intensity or its contrast), that can be modeled by established methods such as simulated annealing, gradient descent, genetic algorithm, etc. [29]. The watershed method has a rich history of success in image segmentation [52–56]. In general, MRI contrast based edges are estimated during image preprocessing and based on the MR image gradients, the contrast edges are merged to define tissue segmentation. Improved watershed methods have been used successfully to segment knee cartilage and normal brain tissues (GM, WM, CSF) with a tissue probability map (prior knowledge) registration [57].

Recently we have used a modified watershed method [58] to detect experimental and human hypoxic ischemic lesions. Initially, a multiparameter calculation was done to compute pixel features such as image contrast edges (by Sobel edge detector [7]), gray-scale intensity values, and mean gradient values of the pixel with its 8-connected neighborhoods (i.e., the local contrast) [7]. These pixel features are considered as the altitudes of the water basin. The water starts at the local maxima and flows along certain paths that have been defined by a genetic algorithm (GA) based energy minimizer to finally reach the local minima [59]. To reduce oversegmentation effects, which are a critical drawback of the watershed method, a similarity based region-merging was then performed. Finally, stroke/ischemic lesions were extracted by utilizing the prior knowledge of mean and standard deviations of stroke regions from MRI, based on similar experimental or clinical neuroimaging data. This process readily detects the ischemic injury in a rodent brain (Fig. 42.4a) and some false positive regions that illustrate the oversegmentation that occurs using the watershed approach.

The GA [59] that was utilized as an energy minimizer in the watershed model [58], allows pixel features (edge, signal intensity, and local contrast) to form an energy topography of the brain MRI. GA starts with a set of randomly selected pixels and iteratively searches for pixels with the lowest variation around it (i.e., pixels with the lowest contrast energy). For any particular iteration, each pixel X is compared with its neighboring pixels and is then replaced by a neighboring pixel Y that is most dissimilar to the original pixel. This process continues until little variation is found in the neighborhood of the pixels contained in the searching set and results in reaching the local energy minima (catchment basins). Small outliers (shallow basins) may contain a few pixels within the current searching set

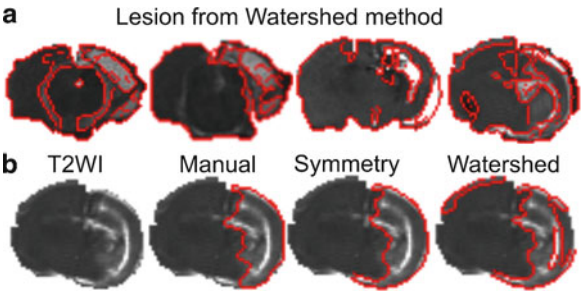

Fig. 42.4 Detection of ischemic injury using the watershed method. (**a**) Ischemic injury in a neonatal rat brain can be detected (*red outline*) with some outlier regions being identified as injured tissues due to oversegmentation inherent in watershed method. (**b**) Comparative results for the symmetry-based and watershed methods along with the manually detected ground-truth ("gold standard") show that the symmetry-integrated approach performs better than the watershed method

but that do not fulfill a trend or criteria (called "fitness" in GA terminology). These outlier pixels are replaced by the same number of new pixels. Replacement is done using random or rule-based techniques that mimic biological evolutionary processes, such as "crossover" (rule-based replacement), "mutation" (random replacement), etc. In this way, the GA based energy minimizer gradually finds the catchment basins from which the watersheds (crests) are computed that segment the medical image into normal and abnormal tissue regions.

Disadvantages of the watershed method include oversegmentation, sensitivity to signal-to-noise ratio (SNR), or poor detection of thin or low SNR brain structures. A comparative example (Fig. 42.4b) illustrates that the modified watershed method detects outliers while the symmetry-integrated method performs much better. In addition, prior information using brain atlases or tissue probability masks can improve segmentation results [57]. However, maturational age-dependence and registration related complexities and uncertainties, specifically in injured brains, may limit the ability of watershed methods in medical image segmentation and lesion detection. Research continues to progress towards solving such limitations.

4 Future Directions in Computational Stroke Assessment

The above overview describes well-established mathematical approaches for the detection of ischemic lesions. Further adaptation could identify signatures within globally injured tissues. While little has been reported, the approaches described below could further delineate tissue level changes.

4.1 Detection of the Ischemic Core and Penumbra

Assessment of salvageable/nonsalvageable tissues and their evolution after a stroke is paramount for candidate selection for therapeutic interventions as well as for monitoring recovery and improving outcome prediction. Tissues within an ischemic lesion are not homogenous. Improved MRI-based estimation of the irreversibly injured core and the potentially salvageable penumbra may lead to better approaches for stroke treatment. Postmortem histology [60] is still considered to be the most reliable method for identifying the core and penumbra but is not clinically applicable. Instead, we have pursued an MRI-based noninvasive estimation of the core/penumbra. We have recently reported in a model of adult rodent ischemia that the expression of the astrocytic marker, glial fibrillary acidic protein (GFAP), was reduced in the penumbra. The penumbra region of interest (ROI) in GFAP pictures was initially localized manually but then confirmed and quantified semiautomatically using manually derived intensity-based threshold, morphological cleaning, then automated volume computation [61]. While we initially used immunohistochemical approaches to identify the penumbra, we sought to extend these studies for use to in vivo neuroimaging.

Current approaches to differentiate the core from penumbra rely on mismatch between diffusion weighted imaging (DWI) and perfusion weighted imaging (PWI) in relevant brain regions and this measure has been used clinically for more than a decade [62, 63]. However, a recent study has detailed several critical drawbacks of this method [64]. When using DWI and PWI, visual (subjective) estimation of the penumbra volume is performed [62, 63], or ROIs detected from one modality are manually traced on the other to estimate the mismatch [65], or manual registration between these two imaging modalities is performed to measure the mismatch [66]. These approaches are neither statistically reliable nor objective. What is required is an automated multimodality coregistration method between DWI and PWI [67]. Previously, one study has proposed T1/T2 lesion differences as possible measure of internal structure of supratentorial lesion [20], but this approach remains limited as it requires multimodality registration and has not been further validated.

We are investigating how variations between MR signal intensity/values within the ischemic/stroke lesion from a single MRI modality (e.g., T2WI or ADC) could discriminate core from penumbra. Because the human eye often cannot distinguish these subtle MR signal variations within the stroke, automated methods such as HRS or SVM (Fig. 42.2a) may be more sensitive, time-saving, and accurate. We have been able to verify our initial automated core/penumbra detection using immunohistochemical validation (Fig. 42.5). In the HRS tree (Fig. 42.1b), we first detect the ischemic lesion and then continue recursive lesion splitting into more uniform subregions. This subdivision allows us to detect the core (higher T2 values) as well as the penumbra (lower T2 values; Fig. 42.1b). The core/penumbra separation is automatically determined from the data based on the actual T2 means of the lesion subregions and prior expert knowledge (Table 42.2). Results from our animal data demonstrate that core/penumbral regions extracted using the HRS method matched

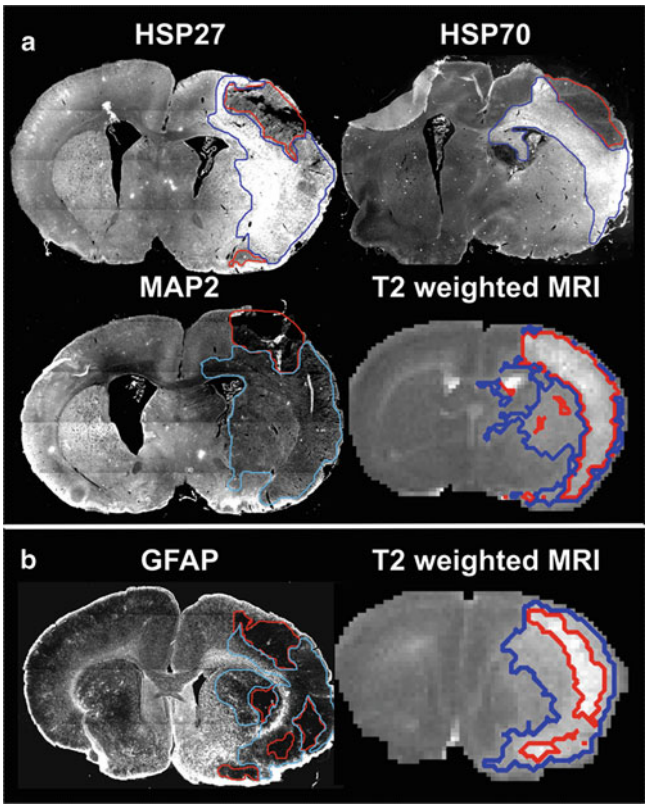

Fig. 42.5 Computational core–penumbra delineation compared to immunohistochemistry. (**a**) HSP27 immunoreactivity (–ir) (*bright region*) and activated HSP70-ir (*bright region*) illustrate the tissue encompassed by the penumbra (see text). Regions of hypointensity (*dark regions*) MAP2 staining reveals the lesion core. The core (*red*) and penumbra (*blue*) detection by HRS on T2WI matches well with corresponding immunohistochemical detections. (**b**) The core (*darkest region*) and penumbra (*less dark area* around the core) manually detected in GFAP stained section also match well with the HRS detected core (*red*) and penumbra (*blue*) in a corresponding T2WI

remarkably well with immunohistochemical staining (Fig. 42.5). We used four molecular markers that have been previously characterized in stroke [60]; (1) heat shock protein 27 (HSP27) is a stress-induced protein that can be found in both astrocytes and neurons within the penumbral tissues, (2) HSP70 (also known as HSP72) is restricted mostly to penumbra tissue, primarily in neurons, (3) glial fibrillary acidic protein (GFAP) as a marker for reactive astrocytes, that are often found in the penumbra, and (4) microtubule associated protein 2 (MAP2) which stains primarily for infarct core tissues and is a global marker for cytoskeletal degradation, independent of cell type.

After semiautomated image registration of immunohistochemical images and MRI of injured brains, good overlap was obtained for the core (sensitivity: 0.60, specificity: 0.95, similarity: 0.83) and the penumbra (sensitivity: 0.59, specificity: 0.89,

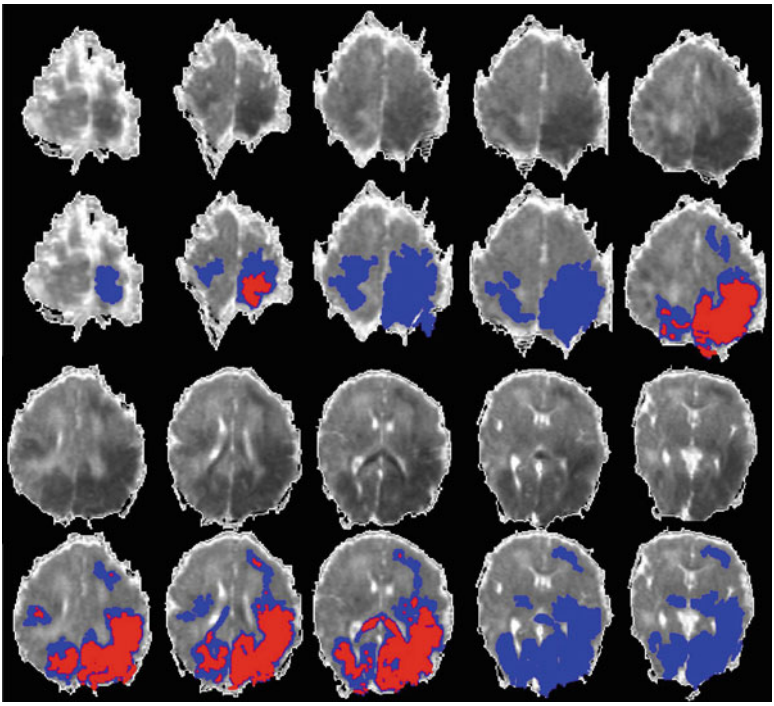

Fig. 42.6 Core–penumbra detection in clinical stroke. HRS based core (*red*) and penumbra (*blue*) detection in a neonatal brain 3 days after stroke. Core regions might be disconnected across consecutive MR slices and a particular MR slice may have only penumbra (*no core*) visible

similarity: 0.65) regions of the ischemic injury [68]. Our findings suggest that HRS has the ability to detect the core/penumbra regions from a single MR modality (as compared to two modalities when DWI/PWI mismatch is used) and also avoids the error prone registration step with DWI/PWI. We performed HRS detection of core/penumbral regions from T2 and ADC maps in several different animal models of ischemia [5, 13]. In addition, we have been able to detect core/penumbra in term neonates suffering from ischemic perinatal stroke (Fig. 42.6).

4.2 Detection of Implanted Stem Cells in Ischemic Brain

Given the current and future interest regarding stem cell therapy, computational approaches to rapidly, objectively and automatically identify these cells in the brain or other organs would have unprecedented utility. We have applied computational approaches to identify neural stem cells (NSCs) implanted following rodent neonatal hypoxia ischemia. NSCs inhibit scar formation, diminish inflammation, promote angiogenesis, provide neurotrophic and neuroprotective support, and stimulate host regenerative processes [2, 69]. Behavioral and anatomical improvements

(lesion volume reduction) after NSC implantation in ischemic brain have been reported [70] and immunohistochemical data have shown that NSCs integrate into injured tissues and develop functionally active connections [70].

To noninvasively monitor implanted NSCs, several labeling techniques have been utilized including, MRI T1-shortening agents (i.e., gadolinium-diethylene triamine pentaacetic acid (Gd-DTPA) labeling) [71], positron emitting isotopes in PET [72], and MRI T2 shortening contrast agents (i.e., Feridex, iron oxide labeling) [73]. We have utilized iron oxide labeling of NSCs to noninvasively visualize these cells as they migrate and replicate in ischemic tissue in translational HII models, even as long as 58 weeks after injury [2, 73]. However, the majority of current NSC detection methods are performed by visual [74] or ad hoc thresholds or templates [15]. NSC locations are currently manually evaluated by observation of MR visible signal voids (iron labeled NSC) at some distance from the implantation site [2]. Reported studies on replication (i.e., proliferation) of NSCs, including our own calculated proliferation index (CPI), also lack region- and cluster-specific quantification [2, 73]. NSC proliferation or replication is defined as an increase in the number of NSCs (quantified by volume and cell density), within a particular NSC cluster over time. However, cellular density cannot be adequately determined using visual methods, hampering true quantitative measurements of replication. Recent studies have attempted to quantify the amount of iron, hence the number of NSCs, using susceptibility weighted images (SWI) and maps [75]. While location is important, the number, density, and replication of these NSCs are equally critical. A recent review on NSC therapy noted that the lack of computational NSC monitoring tools has hindered finding spatiotemporal characteristics of implanted cells [76]. Objective (computational) cellular tracking using feature based matching of NSC clusters (correspondence) at different time points will be required. In addition to NSC volumes, a feature vector developed for individual NSC clusters should contain characteristics that include MR signal intensity or values, 2D/3D shapes, cellular density (measure of signal void), and differences in the gradients of cell density inside (subregions) and outside (gradients across boundary) for each NSC cluster. NSC characteristics (e.g., detectability, density, migration, and replication) will be dependent on their location relative to the HII lesion and the time after implantation. Computational methods could noninvasively quantify and derive the speed/direction of NSC migration, the correlation between migration and cell density variations in NSC clusters, and when, where, and how many NSCs replicate. Such "online" data extraction and analytical approaches are necessary to assure that NSCs have been appropriately implanted, that they remain viable, reach their injury targets, and that host safety after implantation is not compromised.

We have used a deep-rooted HRS tree paradigm (Fig. 42.1b) that can segment very small brain regions based on low kurtosis and low standard deviation values from T2 images and T2 maps. Using previous knowledge (Table 42.2), we reliably detected iron-labeled implanted NSCs from T2WI (Fig. 42.7). Our HRS automated results of NSC detection at and near the implantation site at different imaging time points (Fig. 42.7) are promising and are currently being validated using immunohistochemical staining [77, 78]. We have extended this method to detect iron-labeled NSCs from SWI which we expect will have increased detectability

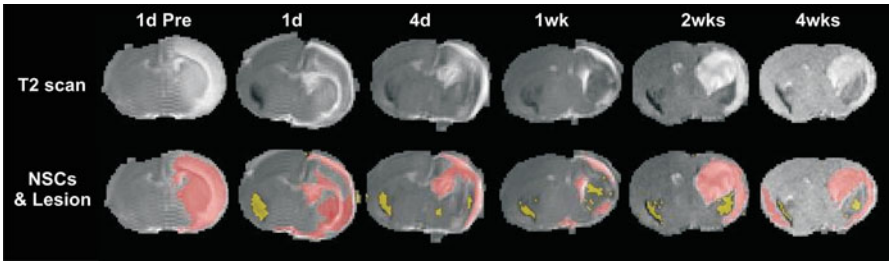

Fig. 42.7 Automatic derivation of NSC and ischemic lesion volumes from MRI. In the Rice-Vanucci model of neonatal ischemia, T2WI were used to delineate normal appearing brain matter, NSCs, and ischemic lesions. The *top row* shows raw T2WI data from serial neuroimaging. The *bottom row* superimposes the HRS extracted lesion (*red*) and NSC (*yellow*) locations onto the T2 maps

due to the exquisite sensitivity of SWI to enhance detection of iron particles within NSCs [75].

4.3 Anatomy-Specific Lesion and Stem Cell Quantification

Stroke within certain anatomical regions (e.g., posterior limb of the internal capsule) can cause significant functional damage, independent of the size of the lesion. In addition, stem cells might have preferential paths in the brain (e.g., through white matter tracts) to reach sites close to the ischemic injury. Better assessment of stroke severity combined with enhanced monitoring of therapeutic interventions could be further strengthened by automated regional and anatomical segmentation. Some treatments may preferentially target cortical or subcortical regions. Specific brain disorders that are known to affect certain anatomical regions (e.g., Parkinson disease) could use an automated atlas or model-based method to minimize false positives. Few studies have been undertaken in this arena.

Previous studies have used brain anatomical templates to first segment brain tissue and then attempt detection of ischemic tissue within these segmented regions [23]. In contrast, we propose a different sequence, whereby the lesions (or implanted cells) are detected first and are then followed by localization based on an anatomical atlas. We believe this would restrict anatomical registration-related errors, as we are not detecting the injury in this step but only quantifying the anatomy-specific proportions of the injured tissues.

Numerous adult brain atlases exist but there are only few available pediatric atlases. A small sample of adult anatomical templates includes: (a) Laboratory of Neuroimaging at the University of California, Los Angeles, CA, USA (http://www.loni.ucla.edu/Atlases/), (b) Biodiversity Bank at Michigan State University, Hickory Corners, MI, USA (https://www.msu.edu/~brains/brains/human/index.html), (c) BrainWeb at MacGill University, Montreal, QC, Canada (http://mouldy.bic.mni.mcgill.ca/brainweb/), and (d) Imperial College, London, UK (http://biomedic.doc.ic.ac.uk/brain-development/index.php?n=Main.Adult). Some pediatric atlases

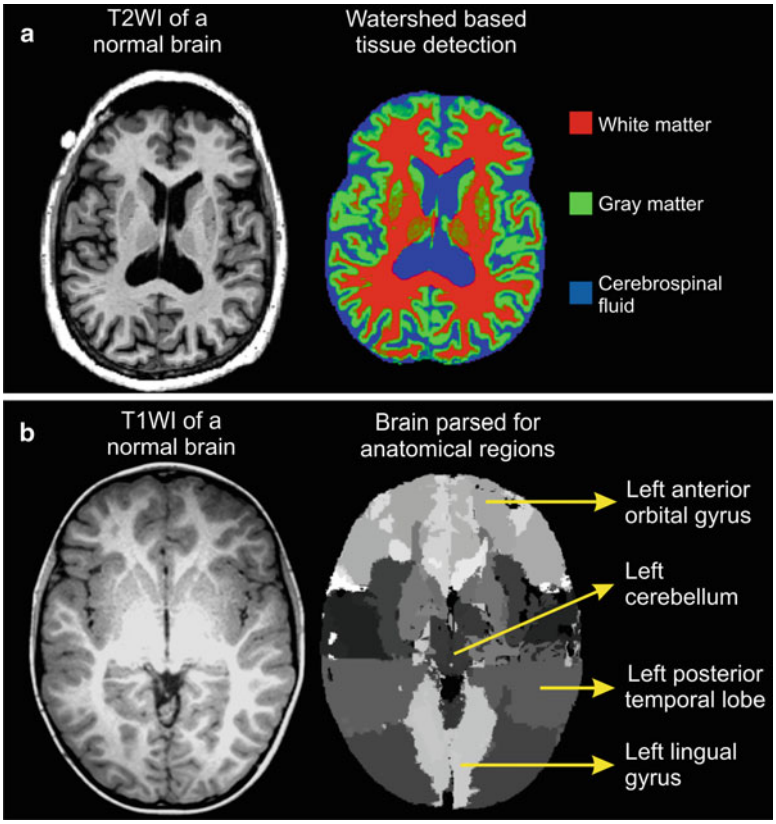

Fig. 42.8 Automated tissue segmentation and anatomical brain parsing. (**a**) Tissue segmentation: The watershed tissue segmentation method of a normal brain MRI into different tissues: white matter (*red*), gray matter (*green*), cerebrospinal fluid (*blue*). Skull-stripping was performed as well. (**b**) Anatomical brain parsing: Anatomical region mapping in an 8-year-old normal pediatric brain using a 2-year-old pediatric brain template from Imperial College, London, UK available online (http://biomedic.doc.ic.ac.uk/brain-development/index.php?n=Main.Neonatal2)

include, (a) Imperial College, London, UK (http://biomedic.doc.ic.ac.uk/brain-development/index.php?n=Main.Neonatal2), (b) Seattle Children's Hospital, Seattle, WA, USA (http://www.seattlechildrens.org/healthcare-professionals/education/radiology/pediatricbrainatlas/), and (c) University of North Carolina, Chapel Hill, NC, USA (https://www.med.unc.edu/bric/ideagroup/free-softwares/unc-infant-0-1-2-atlases).

It is known that one anatomical region may contain multiple tissues (e.g., GM and WM), and injury susceptibility may vary within a single anatomical region also. Thus, anatomical brain parsing results can be further complimented by tissue detections (GM, WM, CSF). We have used our modified watershed method (Sect. 3.4) to extract tissue based segmentation of human brain (Fig. 42.8a). Our automated

registration of a normal 8-year old pediatric brain to a pediatric brain atlas containing 83 brain regions (Imperial College atlas, comprised of 33 two-year old normal children [79]) is illustrated in Fig. 42.8b. Utilizing the Pipeline environment developed by the Laboratory of Neuroimaging at UCLA (http://pipeline.loni.ucla.edu/; [80]) we have found that even without age-matching, anatomical brain regions could be mapped accurately. Beside the already available brain atlases, case-specific atlases can be developed for particular studies to improve computational performance. Such atlases can be generated from age-matched control brains by: (a) coregistering to a standard 3D space, (b) averaging out the individual subtleties, and (c) manually demarking specific brain regions. Such atlases can be developed separately for a particular MR modality (e.g., T2WI, ADC, Diffusion Tensor Imaging, etc.) or images from different modalities can be registered (multimodal registration) to the atlas space (e.g., generally T1/T2 MRI) to acquire anatomical information. Finally, the injured brain can be registered (intra- or intermodality registration) to find region-specific statistical details of the injury. Severe internal or external brain distortions in the diseased brain may create problems with atlas registration, but this can be reduced if only the normal brain areas of the injured brain (after removing the lesion areas) are utilized to compute the image registration matrix [7]. This registration matrix can be used for the entire brain, including injured tissues, for registering it to an atlas followed by extraction of anatomy-specific measures of the injury (or labeled stem cells if implanted).

By using data from core/penumbra regions, GM/WM/CSF tissue regions, and atlas-based brain anatomical localization, one could further extract and quantify region-specific information for the above described data sets, including mean MR values (e.g., T2, ADC, etc.), standard deviations, textures, shapes, kurtosis, skewness, etc. Such detailed complimentary information would be extremely useful in understanding the spatiotemporal evolution of stroke, reparative activities of implanted stem cells and their interactions, and additional therapeutics. These types of assessments cannot be reasonably conducted manually due to the large volume of data and the subjectivity associated with current manual methods.

4.4 Monitoring Spatiotemporal Interactions Between Stroke Tissues and Stem Cells

A final frontier in stroke lesion analysis is automated computation of the process of injury recovery with or without treatment. Beyond simplistic assessment of stem cell volumes, automated algorithms should be able assess stem cell related therapeutic activities such as migration, replication, localization as well as the interaction between the lesion tissues and NSC activities for better understanding of this complex dynamic process. One should be able to determine whether an anatomical region is recovering faster than another, whether the lesion is shifting in the anatomical space, how the MR statistics (e.g., mean, standard deviation) of the lesion changes across anatomy and over time, etc. Despite research using automated

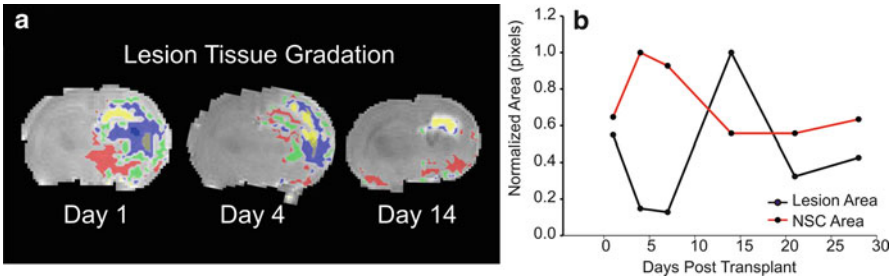

Fig. 42.9 Lesion evolution and interaction. (**a**) Spatiotemporal changes in lesion composition: T2 images from the same RVM rat pup imaged at days 1, 4, and 14 after HII. Each panel shows how the MR values change within the lesion, including the area and shape of the lesion and its subregions over time. Mean T2 relaxation times of the subregions are significantly different: *red* (199 ± 2 ms), *green* (208 ± 3 ms), *blue* (217 ± 3 ms), and *yellow* (231 ± 6 ms). These changes likely reflect different degrees of necrosis/apoptosis and may also reflect differential tissue salvageability. (**b**) Interrelations between temporal evolution of HII lesion and NSC areas. 2D areas of HII lesion and NSC at the same brain level vary over time. The trends are inversely correlated, implying that initially decreasing lesion area gives more viable tissues for NSCs to replicate and as lesion volume increases later, either NSCs die or differentiate into other cells

methods to identify brain lesions, very limited research has considered the importance of the spatiotemporal evolution of the lesion [35]. Kabir and colleagues have qualitatively shown that adult stroke shifts from one anatomical region to other regions without further quantitative evaluation. Estimating or predicting these dynamic changes will expedite advanced monitoring of injury progression and of optimizing treatment strategies.

As ischemic/stroke tissues provide chemoattractive/chemorepulsive cellular and molecular cues [2, 73] combined with differentiation [70] signals to stem cells for injury repair, there is likely a strong interrelationship between these two processes that mutually drive one another. "Toxicity" at the lesional or perilesional regions from dying cells in a compromised vascular microenvironment might be expected to negatively affect NSC viability [2] and we believe that this, as well as the characteristics of homing signals from the lesion, will influence stem cell viability, the extent of cellular migration, replication (i.e., proliferation), and differentiation along with tissue recovery.

Such spatiotemporal interactions are visually and qualitatively reported [81] and the necessity of objective quantification is highlighted in a recent stem cell research review [82]. Our recent work shows that HRS-derived subregions in experimental ischemic lesions (Fig. 42.9a) reveal considerable cellular dynamics in space and time. The HRS method [32] automatically detects ischemic lesions and implanted iron-labeled stem cells (at the implantation site and close to the lesion) over the time course of several weeks (Fig. 42.7). Examining the interaction between injured tissues and stem cell interactions would suggest that stem cell replication is enhanced when lesion volume is reduced (Fig. 42.9b) in the subacute phase (4–5 days after stroke). As the ischemic lesion volume starts to increase toward its final size, stem

cells start to die, presumably due to a more toxic environment. Discovering such patterns using regression analysis or data mining strategies using computational pattern recognition [29] likely will be a key direction for future translational stroke research.

5 Conclusions

Our own studies and those of others suggest that significant advances in computational analytical methods of MRI, CT, and PET data will result in clinically useful applications that have the potential to greatly improve the treatment of children and adults who suffer from focal and global ischemic injuries. The computational approaches we have described provide a glimpse of some of the future directions of automated assessments from imaging data. These approaches with some adaptation can be used for other acute, chronic, and acquired brain injuries.

Acknowledgments Part of this work has been funded by NIH NINDS 1R01NS059770-01A2, National Medical Test Bed (NMTB), LLU Pediatric Research Fund, and an anonymous donation to the Loma Linda University School of Medicine. Part of the research by Drs. Bhanu and Sun has been funded by NSF grants 0641076, 0727129, and 0903667. We are grateful to Dr. Samuel Barnes (LLU) for SVM results, Beatriz Tone and Dr. Hui Rou Tian (LLU) for surgical procedures, Kamal Ambadipudi and Sonny Kim (LLU) for technical assistance with MRI acquisition, Dr. Jerome Badaut (LLU) for use of histochemical equipment, Dr. Evan Y. Snyder (Sanford-Burnham Medical Research Institute, La Jolla, CA, USA) for iron-labeled stem cells, Dr. Ivo Dinov and Dr. Alen Zamanyan (Laboratory of Neuroimaging, UCLA, Los Angeles, USA) for assistance on using LONI Pipeline and brain parsing.

References

1. Ashwal S, Tone B, Tian HR, Chong S, Obenaus A. Serial magnetic resonance imaging in a rat pup filament stroke model. Exp Neurol. 2006;202:294–301.
2. Ashwal S, Obenaus A, Snyder EY. Neuroimaging as a basis for rational stem cell therapy. Pediatr Neurol. 2009;40:227–36.
3. Saunders DE, Clifton AG, Brown MM. Measurement of infarct size using MRI predicts prognosis in middle cerebral artery infarction. Stroke. 1995;26:2272–6.
4. Schiemanck SK, Post MWM, Kwakkel G, Witkamp TD, Kappelle LJ, Prevo AJH. Ischemic lesion volume correlates with long-term functional outcome and quality of life of middle cerebral artery stroke survivors. Restor Neurol Neurosci. 2005;23:257–63.
5. Vannucci RC, Vannucci SJ. Perinatal hypoxic-ischemic brain damage: evolution of an animal model. Dev Neurosci. 2005;27:81–6.
6. Coats JS, Freeberg A, Pajela EG, Obenaus A, Ashwal S. Meta-analysis of apparent diffusion coefficients in the newborn brain. Pediatr Neurol. 2009;41:263–74.
7. Shapiro LG. Stockman GC. Computer Vision: Prentice Hall; 2001.
8. Niimi T, Imai K, Maeda H, Ikeda M. Information loss in visual assessments of medical images. Eur J Radiol. 2007;61:362–6.
9. Barkovich AJ, Westmark K, Partridge C, Sola A, Ferriero DM. Perinatal asphyxia: MR findings in the first 10 days. AJNR Am J Neuroradiol. 1995;16:427–38.

10. Barkovich AJ, Hajnal BL, Vigneron D, Sola A, Partridge JC, Allen F, Ferriero DM. Prediction of neuromotor outcome in perinatal asphyxia: evaluation of MR scoring systems. AJNR Am J Neuroradiol. 1998;19:143–9.
11. Haataja L, Mercuri E, Guzzetta A, Rutherford M, Counsell S, Flavia Frisone M, Cioni G, Cowan F, Dubowitz L. Neurologic examination in infants with hypoxic-ischemic encephalopathy at age 9 to 14 months: use of optimality scores and correlation with magnetic resonance imaging findings. J Pediatr. 2001;138:332–7.
12. Rutherford MA, Pennock JM, Counsell SJ, Mercuri E, Cowan FM, Dubowitz LM, Edwards AD. Abnormal magnetic resonance signal in the internal capsule predicts poor neurodevelopmental outcome in infants with hypoxic-ischemic encephalopathy. Pediatrics. 1998; 102:323–8.
13. Recker R, Adami A, Tone B, Tian HR, Lalas S, Hartman RE, Obenaus A, Ashwal S. Rodent neonatal bilateral carotid artery occlusion with hypoxia mimics human hypoxic-ischemic injury. J Cereb Blood Flow Metab. 2009;29:1305–16.
14. Jiang Q, Zhang ZG, Ding GL, Zhang L, Ewing JR, Wang L, Zhang R, Li L, Lu M, Meng H, Arbab AS, Hu J, Li QJ, Pourabdollah Nejad DS, Athiraman H, Chopp M. Investigation of neural progenitor cell induced angiogenesis after embolic stroke in rat using MRI. Neuroimage. 2005;28:698–707.
15. Mills PH, Wu Y-JL, Ho C, Ahrens ET. Sensitive and automated detection of iron-oxide-labeled cells using phase image cross-correlation analysis. Magn Reson Imaging. 2008;26:618–28.
16. Otsu N. A threshold selection method from gray-level histograms. IEEE Trans Syst Man Cybern. 1979;9:62–6.
17. Flexman JA, Cross DJ, Kim Y, Minoshima S. Morphological and parametric estimation of fetal neural stem cell migratory capacity in the rat brain. Conference Proceedings: Annual International Conference of the IEEE Engineering in Medicine and Biology Society IEEE Engineering in Medicine and Biology Society Conference. 2007; p. 4464–7.
18. Ashwal S, Caots JS, Bianchi A, Bhanu B, Obenaus A. Semi-automated segmentation of ADC maps reliably defines ishchemic perinatal stroke injury. Ecquevilly, France: Sixth Hershey conference on developmental brain injury; 2008.
19. Bricq S, Collet C, Armspach JP. Markovian segmentation of 3D brain MRI to detect multiple sclerosis lesions. Proc of 15th IEEE international conference on image processing (ICIP). San Diego, CA; 2008. p. 733–6.
20. Dugas-Phocion G, Gonzalez MA, Lebrun C, Chanalet S, Bensa C, Malandain G, Ayache N. Hierarchical segmentation of multiple sclerosis lesions in multi-sequence MRI. Proc of IEEE International Symposium on Biomedical Imaging 2007 (ISBI 2007). Arlington, VA, USA; 2007. p. 157–60.
21. Loyek C, Woermann FG, Nattkemper TW. Detection of focal cortical dysplasia in MRI using textural features. Workshop on algorithm, systems and Anwendungen. Berlin: Springer; 2008. p. 432–6.
22. Bergo FPG, Falcao AX, Yasuda CL, Cendes F. FCD segmentation using texture asymmetry of MR-T1 images of the brain. Proc 5th IEEE Intl Symp Biomed Img: from Nano to Macro (ISBI). Paris, France; 2008. p. 424–7.
23. de Boer R, Der Lijn F, Vrooman H, Vernooij M, Ikram M, Breteler M, Niessen W. Automatic segmentation of brain tissue and whitematter lesions in MRI. Proc of IEEE International Symposium on Biomedical Imaging 2007 (ISBI 2007). Arlington, VA; 2007. p. 652–5.
24. Agam G, Weiss D, Soman M, Arfanakis K. Probabilistic brain lesion segmentation in DT-MRI. Proc of IEEE Intl Conf on Image Processing (ICIP). Atlanta Marriott Marquis, Atlanta, GA; 2006. p. 89–92.
25. Freifeld O, Greenspan H, Goldberger J. Lesion detection in noisy MR brain images using constrained GMM and active contours. Proc of IEEE international symposium on biomedical imaging 2007 (ISBI 2007). Arlington, VA; 2007. p. 596–9.
26. Ibrahim M, John N, Kabuka M, Younis A. Hidden Markov models-based 3D MRI brain segmentation. Image Vis Comput. 2006;24:1065–79.

27. Song Z, Tustison N, Avants B, Gee J. Adaptive graph cuts with tissue priors for brain MRI segmentation. Proc of IEEE international symposium on biomedical imaging (ISBI). Arlington, VA; 2006. p. 762–5.
28. He Q, Karsch K, Duan Y. A novel algorithm for automatic brain structure segmentation from MRI. Advances in visual computing. Berlin: Springer; 2008. p. 552–61.
29. Duda RO, Hart PE, Stork DG. Pattern classification. Hoboken: Wiley-Interscience; 2000.
30. Greenspan H, Ruf A, Goldberger J. Constrained Gaussian mixture model framework for automatic segmentation of MR brain images. IEEE Trans Med Imaging. 2006;25:1233–45.
31. Fan L-W, Lin S, Pang Y, Lei M, Zhang F, Rhodes PG, Cai Z. Hypoxia-ischemia induced neurological dysfunction and brain injury in the neonatal rat. Behav Brain Res. 2005;165:80–90.
32. Ghosh N, Recker R, Shah A, Bhanu B, Ashwal S, Obenaus A. Automated ischemic lesion detection in a neonatal model of hypoxic ischemic injury. J Magn Reson Imaging. 2011;33:772–81.
33. Rouainia M, Medjram MS, Doghmance N. Brain MRI segmentation and lesions detection by EM algorithm. Proc of World Academy of Science, Engineering and Technology; 2006. p. 301–4.
34. Yu J, Bhanu B. Super-resolution restoration of facial images in video. Proc of IEEE Intl Conf on pattern recognition (ICPR). Hong Kong, China; 2006. p. 342–5.
35. Kabir Y, Dojat M, Scherrer B, Forbes F, Garbay C. Multimodal MRI segmentation of ischemic stroke lesions. Conference proceedings: annual international conference of the IEEE Engineering in Medicine and Biology Society IEEE Engineering in Medicine and Biology Society Conference; 2007. p. 1595–8.
36. Korb K, Nicholson AE. Bayesian artificial intelligence. Boca Raton, FL: Chapman & Hall; 2003.
37. Chen R, Herskovits EH. A Bayesian network classifier with inverse tree structure for voxel-wise magnetic resonance image analysis. Proceeding of the eleventh ACM SIGKDD international conference. Chicago, IL; 2005. p. 4.
38. Shi J, Malik J. Normalized cuts and image segmentation. IEEE Trans Pattern Anal Mach Intell. 2000;22:888–905.
39. Liao L, Lin T, Li B. MRI brain image segmentation and bias field correction based on fast spatially constrained kernel clustering approach. Pattern Recognition Letters. 2008;29: 1580–8.
40. Nakamura K, Fisher E. Segmentation of brain magnetic resonance images for measurement of gray matter atrophy in multiple sclerosis patients. Neuroimage. 2009;44:769–76.
41. Castellano G, Bonilha L, Li LM, Cendes F. Texture analysis of medical images. Clin Radiol. 2004;59:1061–9.
42. Antel SB, Collins DL, Bernasconi N, Andermann F, Shinghal R, Kearney RE, Arnold DL, Bernasconi A. Automated detection of focal cortical dysplasia lesions using computational models of their MRI characteristics and texture analysis. Neuroimage. 2003;19:1748–59.
43. Dokladal P, Bloch I, Couprie M, Ruijters D, Urtasun R, Garnero L. Topologically controlled segmentation of 3D magnetic resonance images of the head by using morphological operators. Pattern Recognition. 2003;36:2463–78.
44. Prastawa M, Gerig G. Brain lesion segmentation through physical model estimation. Advances in visual computing. Berlin: Springer; 2008 p. 562–71.
45. Kang X, Yund EW, Herron TJ, Woods DL. Improving the resolution of functional brain imaging: analyzing functional data in anatomical space. Magn Reson Imaging. 2007;25:1070–8.
46. Vapnik VN. Statistical learning theory. New York: Wiley-Blackwell; 1998.
47. Lao Z, Shen D, Liu D, Jawad AF, Melhem ER, Launer LJ, Bryan RN, Davatzikos C. Computer-assisted segmentation of white matter lesions in 3D MR images using support vector machine. Acad Radiol. 2008;15:300–13.
48. Saha S, Bandyopadhyay S. MRI brain image segmentation by fuzzy symmetry based genetic clustering technique. Proc of IEEE Cong on evolutionary computation, Singapore; 2007. p. 4417–24.

49. Ray N, Greiner R, Murtha A. Using symmetry to detect abnormalities in brain MRI. Proc Comp Soc Ind Comm. 2008;31:7–10.
50. Sun Y, Bhanu B. Symmetry integrated region-based image segmentation. Proc IEEE Conf on computer vision and pattern recognition (CVPR). Miami, FL; 2009. p. 826–31.
51. Sun Y, Bhanu B, Bhanu S. Automatic symmetry-integrated brain injury detection in MRI sequences. Proc IEEE CVPR workshop on mathematical methods in biomedical image analysis. Miami, FL; 2009. p. 79–86.
52. Beucher S. The watershed transformation applied to image segmentation. Microscopy and Microanalysis: Pfefferkorn Conf on Signal and Image Processing in; 1991.
53. Beucher S, Meyer F. The morphological approach to segmentation: the watershed transform. In: Dougherty ER, editor. Mathematical morphology in image processing. New York, NY: Marcel Dekker; 1993. p. 433–81.
54. Vincent L, Soille P. Watersheds in digital spaces: an efficient algorithm based on immersion simulations. IEEE Trans Pattern Anal Mach Intell. 1991;13:583–98.
55. Nguyen HT, Ji Q. Improved watershed segmentation using water diffusion and local shape priors. Proc IEEE Conf computer vision and pattern recognition. New York, NY; 2006. p. 985–92.
56. Cousty J, Bertrand G, Najman L, Couprie M. Watershed cuts: thinnings, shortest path forests, and topological watersheds. IEEE Trans Pattern Anal Mach Intell. 2010;32:925–39.
57. Grau V, Mewes AU, Alcañiz M, Kikinis R, Warfield SK. Improved watershed transform for medical image segmentation using prior information. IEEE Trans Med Imaging. 2004;23:447–58.
58. Sun Y, Ghosh N, Obenaus A, Ashwal S, Bhanu B. Automated symmetry-integrated brain ROI detection in MRI sequences: a comparison. *IEEE Trans Med Imaging* (TMI) (submitted).
59. Bhanu B, Lee S. Genetic learning for adaptive image segmentation. Boston, MA: Kluwer; 1994.
60. Popp A, Jaenisch N, Witte OW, Frahm C. Identification of ischemic regions in a rat model of stroke. PLoS One. 2009;4:e4764.
61. Titova E, Ostrowski RP, Adami A, Badaut J, Lalas S, Ghosh N, Vlkolinsky R, Zhang JH, Obenaus A. Brain irradiation improves focal cerebral ischemia recovery in aged rats. J Neurol Sci. 2011;306:143–53.
62. Wechsler LR. Imaging evaluation of acute ischemic stroke. Stroke. 2011;42:S12–5.
63. Olivot J-M, Albers GW. Diffusion-perfusion MRI for triaging transient ischemic attack and acute cerebrovascular syndromes. Curr Opin Neurol. 2011;24:44–9.
64. Wardlaw JM. Neuroimaging in acute ischaemic stroke: insights into unanswered questions of pathophysiology. J Intern Med. 2010;267:172–90.
65. Straka M, Albers GW, Bammer R. Real-time diffusion-perfusion mismatch analysis in acute stroke. J Magn Reson Imaging. 2010;32:1024–37.
66. Schlaug G, Benfield A, Baird AE, Siewert B, LÃvblad KO, Parker RA, Edelman RR, Warach S. The ischemic penumbra: operationally defined by diffusion and perfusion MRI. Neurology. 1999;53:1528–37.
67. Ma H, Zavala JA, Teoh H, Churilov L, Gunawan M, Ly J, Wright P, Phan T, Arakawa S, Davis SM, Donnan GA. Penumbral mismatch is underestimated using standard volumetric methods and this is exacerbated with time. J Neurol Neurosurg Psychiatry. 2009;80:991–6.
68. Ghosh N, Turenius CI, Tone B, Snyder EY, Obenaus A, Ashwal S. Automated core-penumbra quantification in neonatal ischemic brain injury. Stroke (submitted).
69. Singec I, Jandial R, Crain A, Nikkhah G, Snyder EY. The leading edge of stem cell therapeutics. Annu Rev Med. 2007;58:313–28.
70. Park KI, Himes BT, Stieg PE, Tessler A, Fischer I, Snyder EY. Neural stem cells may be uniquely suited for combined gene therapy and cell replacement: evidence from engraftment of neurotrophin-3-expressing stem cells in hypoxic-ischemic brain injury. Exp Neurol. 2006;199:179–90.
71. Adler ED, Bystrup A, Briley-Saebo KC, Mani V, Young W, Giovanonne S, Altman P, Kattman SJ, Frank JA, Weinmann HJ, Keller GM, Fayad ZA. In vivo detection of embryonic stem

cell-derived cardiovascular progenitor cells using Cy3-labeled Gadofluorine M in murine myocardium. JACC Cardiovasc Imaging. 2009;2:1114–22.
72. Qiao H, Zhang H, Zheng Y, Ponde DE, Shen D, Gao F, Bakken AB, Schmitz A, Kung HF, Ferrari VA, Zhou R. Embryonic stem cell grafting in normal and infarcted myocardium: serial assessment with MR imaging and PET dual detection. Radiology. 2009;250:821–9.
73. Obenaus A, Dilmac N, Tone B, Tian HR, Hartman R, Digicaylioglu M, Snyder EY, Ashwal S. Long-term magnetic resonance imaging of stem cells in neonatal ischemic injury. Ann Neurol. 2011;69:282–91.
74. Guzman R, Bliss T, De Los Angeles A, Moseley M, Palmer T, Steinberg G. Neural progenitor cells transplanted into the uninjured brain undergo targeted migration after stroke onset. J Neurosci Res. 2008;86:873–82.
75. Kressler B, de Rochefort L, Liu T, Spincemaille P, Jiang Q, Wang Y. Nonlinear regularization for per voxel estimation of magnetic susceptibility distributions from MRI field maps. IEEE Trans Med Imaging. 2009;29:273–81.
76. Kraitchman DL, Gilson WD, Lorenz CH. Stem cell therapy: MRI guidance and monitoring. J Magn Reson Imaging. 2008;27:299–310.
77. Ghosh N, Turenius CI, Tone B, Obenaus A, Ashwal S. MRI-based automated monitoring of activities of implanted stem cells in neonatal ischemic injury. Ann Neurol (submitted).
78. Turenius CI, Ghosh N, Dulcich M, Denham CM, Tone B, Hartman R, Snyder EY, Obenaus A, Ashwal S. Iron toxicity and gender based study of implanted hNSC in neonatal ischemic injury. Exp Neurol (submitted).
79. Gousias IS, Rueckert D, Heckemann RA, Dyet LE, Boardman JP, Edwards AD, Hammers A. Automatic segmentation of brain MRIs of 2-year-olds into 83 regions of interest. Neuroimage. 2008;40:672–84.
80. Dinov ID, Van Horn JD, Lozev KM, Magsipoc R, Petrosyan P, Liu Z, Mackenzie-Graham A, Eggert P, Parker DS, Toga AW. Efficient, distributed and interactive neuroimaging data analysis using the LONI pipeline. Front Neuroinform. 2009;3:22.
81. Faiz M, Acarin L, Villapol S, Schulz S, Castellano B, Gonzalez B. Substantial migration of SVZ cells to the cortex results in the generation of new neurons in the excitotoxically damaged immature rat brain. Mol Cell Neurosci. 2008;38:170–82.
82. Kim D, Hong KS, Song J. The present status of cell tracking methods in animal models using magnetic resonance imaging technology. Mol Cells. 2007;23:132–7.